Collective protection against the type VI secretion system in bacteria

Elisa T. Granato*[1,2], William P. J. Smith* [1,2,3], Kevin R. Foster[1,2]

*Equal contribution

[1] Department of Biology, University of Oxford, Oxford, UK

[2] Department of Biochemistry, University of Oxford, Oxford, UK

[3] Division of Genomics, Infection and Evolution, University of Manchester, UK

ABSTRACT

Bacteria commonly face attacks from other strains via the type VI secretion system (T6SS), a molecular speargun that stabs and intoxicates competitors. Here we show how bacteria can work together to collectively defend themselves against these attacks. This project began with an outreach activity: while developing an online computer game of bacterial warfare, we noticed that one strategist ("Slimy") that made extracellular polymeric substances (EPS) was able to resist attacks from another strategist that employed the T6SS ("Stabby"). This observation motivated us to model this scenario more formally, using dedicated agent-based simulations. The model predicts that EPS production can serve as a collective defence mechanism, which protects both producing cells and neighbouring cells that do not make EPS. We then tested our model with a synthetic community that contains a T6SS-wielding attacker (*Acinetobacter baylyi*), and two T6SS-sensitive target strains (*Escherichia coli*) that either secrete EPS, or not. As predicted by our modelling, we find that the production of EPS leads to collective protection against T6SS attacks, where EPS producers can shield each other and nearby non-producers. Our work shows how EPS-producing bacteria can work together to defend themselves from attackers.

INTRODUCTION

Bacteria commonly live in densely-populated, multispecies communities where they must compete for limited space and nutrients (1–3). Life in these environments has driven the evolution of an array of bacterial weapon systems, used to inhibit or kill competing microbes (4, 5). One of the most widespread and sophisticated of these weapons is the type VI secretion system (T6SS), a contractile nanomachine that fires a needle into neighbouring bacteria to deliver toxic effector proteins (6).

Possession of the T6SS can confer a strong ecological advantage to bacteria cells (7–10). Conversely, being on the receiving end of a T6SS attack can be lethal. Defending against the T6SS, however, presents a unique set of problems for targeted cells, as—unlike many other weapon systems—the T6SS does not rely on the target cell's surface receptors or transport systems. Instead, it uses mechanical force to pierce the target cell's membrane and deliver its toxic cargo, which limits the potential range of mechanisms that can be employed in defence (11).

In the face of these challenges, here we show how bacteria can work together to protect themselves against T6SS attacks. Individual-level defence mechanisms are known, including immunity proteins, capsule formation, target modification, envelope stress responses, and the removal of susceptibility factors (12–16). However, some of the most powerful defences in bacteria come about when bacteria act as a collective, allowing groups of cells to take advantage of their large numbers (17–22).

This project began when we serendipitously identified a potential collective defence mechanism against the T6SS while developing a video game, as part of an outreach activity. The game—*Gut Wars*—uses an agent-based model developed by our group for research (17, 23–25) to illustrate different bacterial warfare strategies in the human gut microbiome. Running the game repeatedly, we noticed that "Slimy" strategists, which secrete extracellular polymeric substances (EPS), were particularly resistant against "Stabby" competitors armed with the T6SS. Secretion of EPS is widespread among bacteria and plays a key role in the formation of biofilms (26, 27). Unlike typical anti-T6SS defence mechanisms that act at the level of the individual cell, we saw that EPS released into the environment has the potential to protect both the cell that produces it and others around it, thereby functioning as a powerful collective defence mechanism. There is evidence that EPS has the potential to be physically resistant to T6SSs (12, 13, 15). Moreover, biofilm formation—involving EPS secretion—is known to reduce T6SS susceptibility (14), and is a

response to bacterial competition via T6SS (28). We, therefore, decided to investigate whether EPS allows bacteria to work collectively in the face of T6SS attacks.

Here, we develop agent-based models of the competitions between T6SS attackers and EPS-producing target cells. As suggested by the computer game, these analyses predict that secreting EPS is a collective defence mechanism in which producer cells both protect each other, and also cross-protect nearby non-producing cells. We test our predictions using a synthetic community, in which T6SS-wielding *Acinetobacter baylyi* are competing with *Escherichia coli* strains secreting free (i.e. non-membrane-bound) EPS in amounts comparable to clinical *E. coli* isolates. These experiments revealed that EPS can indeed serve as a powerful collective defence against T6SS attacks.

RESULTS

Agent-based modelling predicts that EPS can protect against T6SS

Bacteria have evolved a wide repertoire of traits and strategies to increase their survival chances in densely-populated communities. We recently devised a simple browser-based computer game—*Gut Wars*—to showcase some of these competition strategies in a format accessible to children as well as adults. The game asks the user to select different characters representing distinct bacterial competition strategies, which are then pitted against each other in a simulated gut microbiome environment using agent-based modelling (Fig. 1A). Two of the available strategies are EPS production ("Slimy") and T6SS firing ("Stabby"), both common traits in bacteria. While not originally implemented to fulfil this function, we noticed that i) "Slimy" bacteria were surprisingly resistant to T6SS attacks, and ii) the simulated EPS particles covered a large area around the producing cells. This led us to ask whether the secretion of loose (i.e. non-membrane-bound) EPS could protect cells from T6SS firing events, and so help EPS-producing bacteria survive when faced with a T6SS attacker.

To explore these questions, we implemented EPS secretion within an existing individual-based model of T6SS competition (24, 25). Following previous models (29–31), EPS production is modelled as cells secreting loose, spherical particles into the environment, at a rate P_{EPS} (see Materials and Methods). As they grow, divide, and secrete EPS, producing cells create small pockets of EPS particles around themselves, which helps to separate cells from T6SS-wielding competitors (Fig. 1B). Note, we do not assume here that EPS can physically block T6SS needles,

as this effect may not be universal (15). However, were this to occur, the expectation is that it will only increase the protection conferred to cells.

We performed simulation parameter sweeps to identify conditions where EPS production was most protective against T6SS attacks. Comparing simulations with and without EPS (respectively, P_{EPS} = 0.1, 0), we used a simple metric to quantify the benefit of EPS protection:

$$\textit{EPS benefit} = (N_{susc}(t_{end}) / N_{susc}(t_{start}))_{EPS+} - (N_{susc}(t_{end}) / N_{susc}(t_{start}))_{EPS-} ,$$

with $N_{susc}(t)$ the number of surviving susceptible cells present at time t. Varying the starting number of attacker and susceptible cells shows that EPS production always offers at least some T6SS protection (*EPS benefit* > *0*), and that production is most beneficial for intermediate attacker- and susceptible cell densities (Fig. 1C).

We performed additional simulations to test the robustness of EPS-mediated T6SS protection with respect to other simulation parameters (Fig. S1). Repeats of competition simulations with different EPS production rates showed that, as might be expected, susceptible survival decreases as the per-cell rate of EPS secretion is reduced (Fig. S1A); below a minimal secretion rate, survival is indistinguishable from that of a non-producing susceptible strain. We also tested a model in which EPS production is costly, such that susceptible cells suffer a growth penalty proportional to their EPS production rate,

$$\textit{Susceptible growth rate} = k_{grow}(1 - c_{EPS}\, P_{EPS}),$$

with k_{grow} the maximum cell growth rate, P_{EPS} the probability of EPS secretion per simulation timestep, and c_{EPS} the unit cost of EPS production. For various $c_{EPS} > 0$, costly EPS production remains net-beneficial to susceptible cells (Fig. S1B), such that the optimal secretion rate $P_{EPS}^* >$ 0. Predictably, EPS investment collapses for excessive costs (Fig. S1B), and is contingent on attacker presence (Fig. S1C). Overall, our simulations predict that production of loose, non-membrane-bound EPS is an effective means for cells to protect themselves against the T6SS, even when costly.

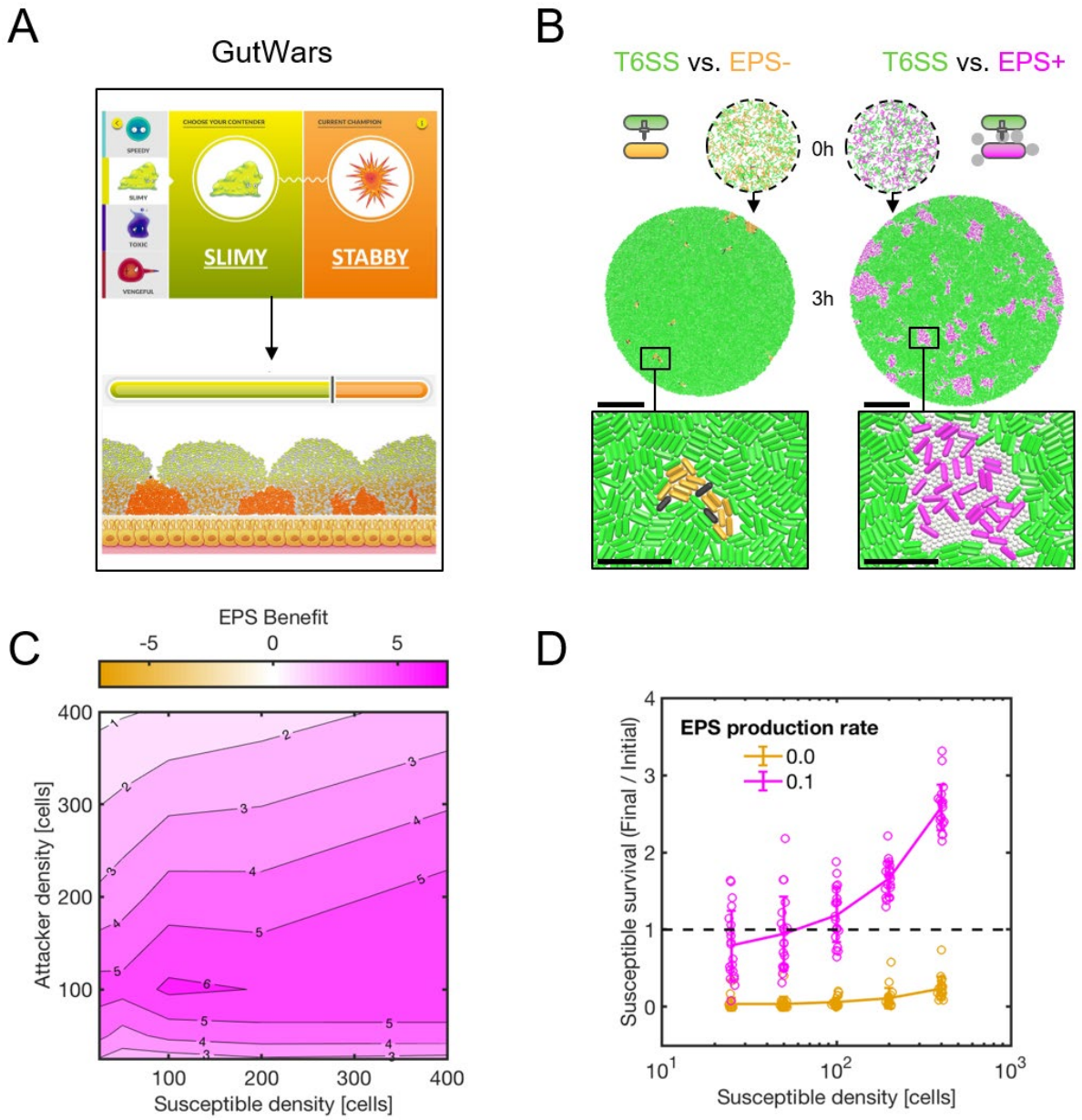

Fig. 1: Agent-based modelling of EPS secretion demonstrates collective defence against the T6SS. **(A)** Snapshots of our agent-based video game 'GutWars', showing EPS-producing 'Slimy' bacteria outcompeting T6SS-armed 'Stabby' rivals. **(B)** Agent-based simulations compete T6SS attackers (green) with EPS non-producing (EPS-, P_{EPS} = 0.0) and EPS-producing (EPS+, P_{EPS} = 0.1) susceptible cells (orange and magenta, right and left columns, respectively). Snapshots show i) initial cell seeding (0h), with 400 cells of each type scattered within a circular homeland, and ii) cell configuration after 3 hours' competition (3h). Scale bars: 50 µm. Zoomed sections highlight dead (black) susceptible cells and distribution of EPS particles. Inset scale bars: 10 µm. **(C)** Contour plot showing measurements of mean EPS benefit (see main text) as a function of initial attacker and susceptible cell density. N=20 simulation replicates per parameter combination. **(D)** Plot showing susceptible final:initial cell counts against initial susceptible density, exemplifying density-dependent benefit of EPS production (fixed attacker density of 400 cells). Individual data points are shown; lines and error bars correspond to data means and standard deviations. Dashed line denotes Final:Initial susceptible ratio = 1, i.e. no net loss or gain of susceptible strain. N=20 simulation replicates per parameter combination; data replotted from (C).

120 **EPS protection is predicted to function as a collective trait**

121 We next used the simulations to more formally evaluate whether EPS protection is a collective
122 trait. A key feature of many collective traits is a positive relationship between the number of
123 individuals with the trait, and the benefit conferred (32). To look for this, we plotted the benefit of
124 EPS production against the starting number of susceptible (EPS producer) cells, which revealed
125 that the relationship is positive for many levels of EPS secretion (Fig. 1D, S2A, S2B). Note that
126 our metric controls for any density-dependent survival effects emerging solely from changes to
127 cell group size (33). That is, while survival is expected to generally increase with susceptible cell
128 number, this effect becomes much stronger when susceptible cells also produce EPS (Fig. 1D).
129

130 Next, we examined the extent to which the benefits from EPS production are shared among cells,
131 which is a second key feature of collective traits. Using the same competition protocol as before,
132 we ran simulations pitting T6SS attackers against susceptible EPS- cells, susceptible EPS+ cells,
133 or both together (Fig. 2A), for a range of initial cell densities. We then quantified the survival of
134 both the EPS+ cells and the EPS- cells when they grew either i) alone with the attacker or ii)
135 paired with the other susceptible cell type (Fig. 2B). As expected when the protective effect of
136 EPS is shared between cells, EPS- survival increased in the presence of EPS+ cells (Fig. 2B,
137 'rescue'), and, conversely, EPS+ survival decreased in the presence of EPS- cells (Fig. 2B,
138 'exploitation').
139

140 **A synthetic community demonstrates collective protection via EPS**

141 To test the model's predictions empirically, we turned to an established experimental system for
142 studying T6SS killing: competitions between a T6SS+ *A. baylyi* attacker strain and a T6SS-
143 susceptible *E. coli* strain (MG1655; (34)). Using their T6SS, *A. baylyi* cells can inject a cocktail of
144 different effector proteins into neighbouring cells which rapidly induce lysis in susceptible *E. coli*
145 (24). To compare the relative T6SS susceptibility of EPS-producing and non-producing *E. coli*,
146 we created *E. coli* MG1655 pRcsA2 (EPS+), a strain capable of undergoing IPTG-inducible
147 production of the exopolysaccharide colanic acid, which is a major component of natural *E. coli*
148 biofilms (35, 36). Colanic acid production is induced via plasmid-based expression of RcsA, the
149 major positive regulator of colanic acid biosynthesis in *E. coli* (37). Its plasmid-free parent
150 MG1655 serves as the non-EPS-producing control strain (EPS-), as MG1655 does not produce
151 significant amounts of colanic acid under the conditions used in this study (Fig. S3).

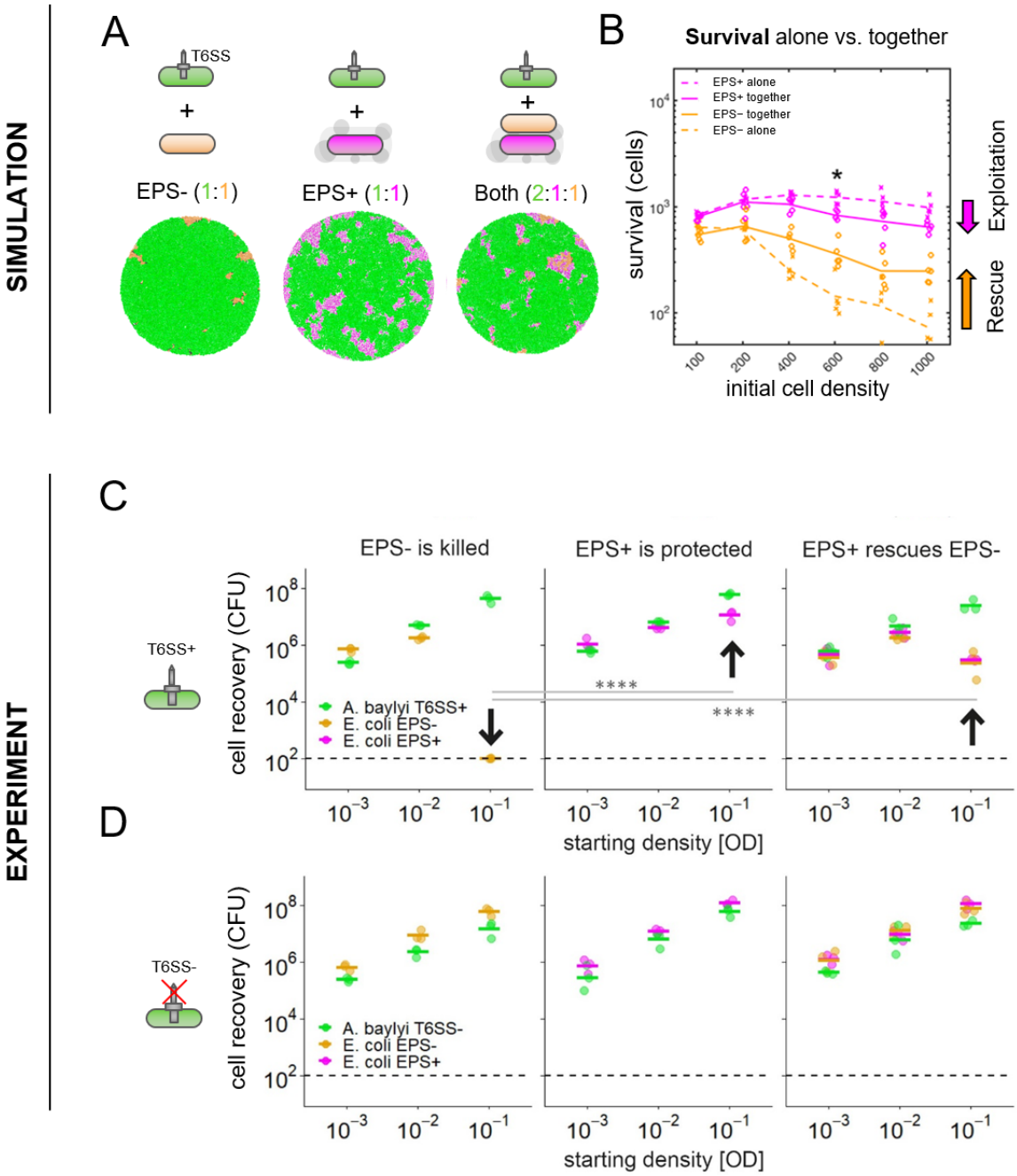

Fig. 2: Modelling and experiments show that EPS secretion protects both producer and non-producer *E. coli* from T6SS attacks. (A) End-state snapshots of agent-based simulations competing T6SS attackers (green) with EPS- or EPS+ (orange, magenta) strains, or both strains at once. **(B)** Survival of each susceptible strain (EPS+, magenta; EPS-, orange) growing alone against T6SS attackers (dashed lines), or together with the other susceptible strain type (solid lines). * denotes the scenario depicted in (A). **(C+D)** We conducted analogous competition assays *in vitro* between three bacterial strains: *A. baylyi* ADP1 (T6SS attacker), *E. coli* MG1655 Gen^R (EPS-), and *E. coli* MG1655 pRcsA2 (EPS+; colanic acid overproducer). For each strain, cell recovery (CFU) after 6h of co-culturing at different starting cell densities (optical density; OD) is shown. Individual data points (n=3) and their means are shown as dots and lines, respectively. Arrows highlight key comparisons. **(C)** Survival of *E. coli* EPS- (left), EPS+ (centre) or a 1:1 mix of EPS- and EPS+ (right), when competed against T6SS+ *A.*

baylyi. At high seeding density (OD = 10^{-1}), EPS+ cells survive pairwise competitions against a T6SS attacker better than EPS- cells (middle and left; $p < 0.0001$). When co-cultured with EPS+ and competing against the attacker (right), survival of EPS- cells is strongly increased relative to when they face the attacker alone (left; $p < 0.0001$). When EPS+ cells are co-cultured with EPS- and compete against the attacker (right), EPS+ survival is reduced compared to when they face the attacker alone (left; $p < 0.0001$). **(D)** Repeat of (C) with *A. baylyi* lacking a functional T6SS. When competed against a T6SS- attacker in pairwise competitions, no difference in cell recovery between EPS+ and EPS- cells was detected ($p = 0.66$). For both (C) and (D), competitions were analysed per strain combination and seeding density, with statistical analyses on log-transformed data via two-way ANOVA ($\alpha = 0.01$) with Tukey post-hoc tests (****: $p < 0.0001$).

152 We first sought to measure the amount of colanic acid secreted by the EPS+ strain, as well as
153 test where it is localised with respect to the cell membrane. Across *E. coli* strains, colanic acid
154 can be secreted both as a capsule tethered to the producing cell membrane, as well as in
155 untethered, loose form (38). The difference between these two states is likely to strongly influence
156 the role of colanic acid in collective protection from external assaults. To benchmark our colanic
157 acid quantification and localization assays, we compared the EPS+ and EPS- strains to six clinical
158 *E. coli* isolates (Table S2). As for the majority of the clinical isolates, phase-contrast microscopy
159 showed that our EPS+ strain has no visible membrane-bound capsule. This observation is
160 consistent with colanic acid being untethered to producing cells and released into the extracellular
161 environment (Fig. S3A). This conclusion was further supported by colanic acid quantification
162 assays where we measured the amount of colanic acid found in total cell extracts vs. supernatant
163 fractions of cultures harvested from agar plates. For the EPS+ strain, the entirety of the detected
164 colanic acid was recovered in the supernatant (Fig. S3B). This same assay also revealed that the
165 amount of loose colanic acid secreted by EPS+ is comparable to that secreted by two clinical
166 isolates (#0172 and #0993, Fig. S3B). The EPS+ *E. coli* strain, therefore, secretes loose colanic
167 acid at rates comparable to naturally occurring *E. coli,* allowing for a direct test of the role of EPS
168 in T6SS-mediated competitions.
169
170 Next, we compared the EPS+ and EPS- *E. coli* strains in competition against a T6SS-wielding *A.*
171 *baylyi* (ADP1; T6SS+) and a T6SS-deficient mutant (ADP1 Δ*tssM*; T6SS-). We seeded a 1:1
172 mixture of *A. baylyi* with either EPS+ or EPS- *E. coli* at various densities on agar plates and
173 measured strain recovery after 6h of co-culture using selective plating (Fig. 2C). At low seeding
174 densities, the T6SS is less efficient because it relies on cell-cell-contact for killing (24, 33). At high
175 seeding densities, we expect the T6SS to be maximally effective; this was confirmed in our
176 competition assays, as the EPS- control strain suffered maximal killing at high densities (Fig. 2C,
177 left). In contrast, the EPS+ strain survived much better at high densities (Fig. 2C, middle), with a
178 10^5-fold increase in survival against T6SS+ *A. baylyi* compared to EPS-. This advantage was

179 dependent on T6SS-activity, as there was no detectable difference in recovery between EPS+
180 and EPS- after pairwise competition with the T6SS- *A. baylyi* (Δ*tssM*) mutant (Fig. 2D). To test
181 whether the presence of EPS in the environment alters T6SS activity, we measured firing rates in
182 hundreds of T6SS+ *A. baylyi* cells exposed to cell-free supernatants with and without EPS, and
183 were unable to detect a difference (Fig. S4). These results strongly support our model's prediction
184 that non-membrane-bound EPS can protect susceptible cells from killing by the T6SS.
185
186 We then examined the potential for a producer strain to cross-protect a non-producer, as expected
187 for a collective defence mechanism. We conducted 3-way competitions between T6SS+ *A. baylyi*
188 and both the EPS+ and EPS- *E. coli* (2:1:1 ratio of *A. baylyi* : EPS+ : EPS-) and quantified strain
189 recovery as above. At high seeding densities, as predicted by the model, the survival of EPS-
190 increased 1000-fold in the presence of EPS+ (Fig. 2C, right) compared to when they faced the
191 T6SS attacker alone (Fig. 2C, left), indicating that the presence of secreted EPS can rescue
192 otherwise susceptible cells from T6SS attacks even if they do not produce EPS themselves.
193 Further consistent with the modelling, we observed that relative survival of the EPS+ strain
194 decreased in presence of EPS- (Fig. 2C, right) compared to when grown alone with the T6SS
195 attacker (Fig. 2C, left) suggesting that the presence of non-producing cells partially compromises
196 the protective effects of EPS production.
197
198 **Cross-protection can emerge from flank protection**
199 Our modelling and experiments show that EPS can function as a collective defence, whose
200 benefit is shared among cells in a colony or biofilm. We next sought to understand the
201 mechanism(s) underpinning this collective property. We initially reasoned that loose EPS would
202 be shared between cells, resulting in the protection of non-producing cells seen in both modelling
203 and experiments. To test this hypothesis, we modified our model so that EPS+ cells no longer
204 secreted loose EPS particles, but instead became intrinsically resistant to T6SS attacks (requiring
205 2 hits to kill instead of 1), as has been demonstrated in capsule-forming bacteria (15). The goal
206 of this model was to remove the possibility of EPS sharing between cells, so that we could test
207 whether sharing was necessary for the cross-protection of non-producer cells (Fig. 3).

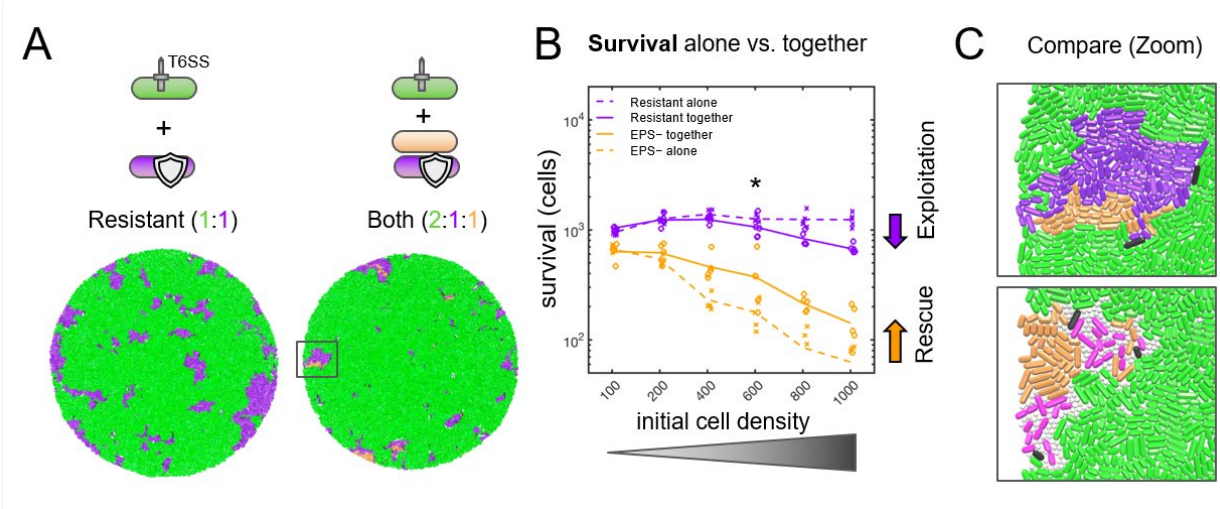

Fig. 3. Modelling shows that cross protection can occur without EPS sharing (A) End-state snapshots of agent-based simulations competing T6SS attackers (green) with an EPS- strain (orange), a T6SS-resistant strain (purple) that secretes no EPS particles, or both strains at once. Box corresponds to zoomed section in (C). **(B)** Survival of Resistant strain (purple) and the EPS- susceptible strain (orange) growing alone against T6SS attackers (dashed lines), or together with the other strain type (solid lines). N=5 simulations per parameter combination; lines denote mean survival. **(C)** Magnified views showing Resistant strain shielding EPS- from the attacker (top), similar to where protection occurs via secretion of loose EPS (bottom).

We then competed the resistant cell type against T6SS attackers as before, either in the presence or absence of the EPS- susceptible cell type (Fig. 3A). To our surprise, this again lead to collective T6SS defence, which displayed both cross-protection and the same density-dependence seen for loose EPS (Fig. 3B). Close inspection of simulations revealed that resistant cells act as barriers, protecting the flanks of susceptible cell groups by physically separating them from T6SS attackers (Fig. 3C). We therefore term this mechanism ‘flank protection’. Because we see cross protection, flank protection is also a collective effect, but one that can be provided by a purely private resistance mechanism, as well as by loose EPS.

Time-lapse microscopy demonstrates cross-protection involves EPS sharing

Our modelling shows that EPS-producing bacteria can collectively defend themselves against T6SS attacks via flank protection, without sharing of EPS between cells. However, an important simplification of the model is that it represents EPS as small solid spheres. This limits the ability of EPS to flow past and around cells in a manner that may not always reflect the behaviour of real EPS (39). Given this potential limitation of the model, we decided to investigate whether our original hypothesis of EPS sharing was important in the experimental data, even if it was not necessary for collective defence in the model. To do this, we turned to time-lapse confocal microscopy, which enables direct observation of cells over time (Fig 4). We competed fluorescent

226 protein-expressing strains of *A. baylyi* (*vipA-sfGFP*, green) with EPS+ *E. coli* (*mScarlet*, magenta)
227 and EPS- *E. coli* (*BFP*, orange) and performed competitions on agar pads as before, except we
228 imaged different locations in the competition area hourly, using confocal microscopy. End-state
229 images of the competition area (Fig. 4A) provided visual confirmation of i) improved survival of
230 EPS+ relative to EPS-, and ii) improved survival of EPS- in the presence of EPS+. Surviving EPS-
231 cells also tended to co-localise with EPS+ cells (bottom right), similar to behaviour observed in
232 our model.
233
234 To look for signatures of EPS-mediated cross-protection in our time-lapse data, we examined
235 T6SS-mediated killing at boundaries between *A. baylyi* and *E. coli* cell groups (Fig. 4B) using
236 automated analysis of confocal time-lapse images. We reasoned that, if cross-protection occurred
237 via the association of loose EPS with EPS- cells, then an EPS- cell group should be able to
238 withstand the T6SS attacker better when EPS+ producers were also present. Specifically, the
239 boundaries between the T6SS attacker and EPS- cells should shift less in the favour of the T6SS
240 attacker, if EPS+ cells are also present nearby. Accordingly, we measured the rate of *A. baylyi*
241 encroachment into EPS+ and EPS- cell groups (Fig. 4B, “Invasion”), normalising this by the total
242 length of interface between *A. baylyi* and each individual susceptible strain (Fig. 4B, “Boundary”).
243 The resulting metric, which we term the normalised invasion rate, provides an estimate of how
244 susceptible each *E. coli* strain is to T6SS attack. Crucially, since the normalised invasion rate
245 examines *A. baylyi*–EPS+ and *A. baylyi*–EPS- strain interactions separately, it excludes any
246 possible effects of flank protection.
247
248 Our measurements of normalised invasion rates over time showed that the EPS- strain was
249 indeed invaded less rapidly when grown together with the EPS+ strain, vs. when grown alone
250 (Fig. 4C, left). This improvement was most pronounced between hours 3 and 4 of competition.
251 Meanwhile, the EPS+ strain was invaded at a consistently lower rate (Fig. 4C right) than the EPS-
252 strain, with normalised invasion rates largely unchanged by the presence / absence of the EPS-
253 strain (i.e., no significant exploitation effect detected). These effects are summarised in Fig. 4D:
254 integrating over all time points, the EPS- cell groups suffered significantly more invasion when
255 the EPS+ strain was absent. Importantly, this variation was contingent on T6SS activity: control
256 experiments showed minimal variation in EPS- strain invasion with EPS+ strain presence when
257 attackers lacked a functional T6SS (Fig. 4E, right). Note that these data do not exclude a role for
258 flank protection in the experiments, but they do provide evidence that EPS+ cells increase survival

259 of EPS- cells *at a distance*. This result is consistent with collective protection being mediated—at
260 least in part—by shared EPS.

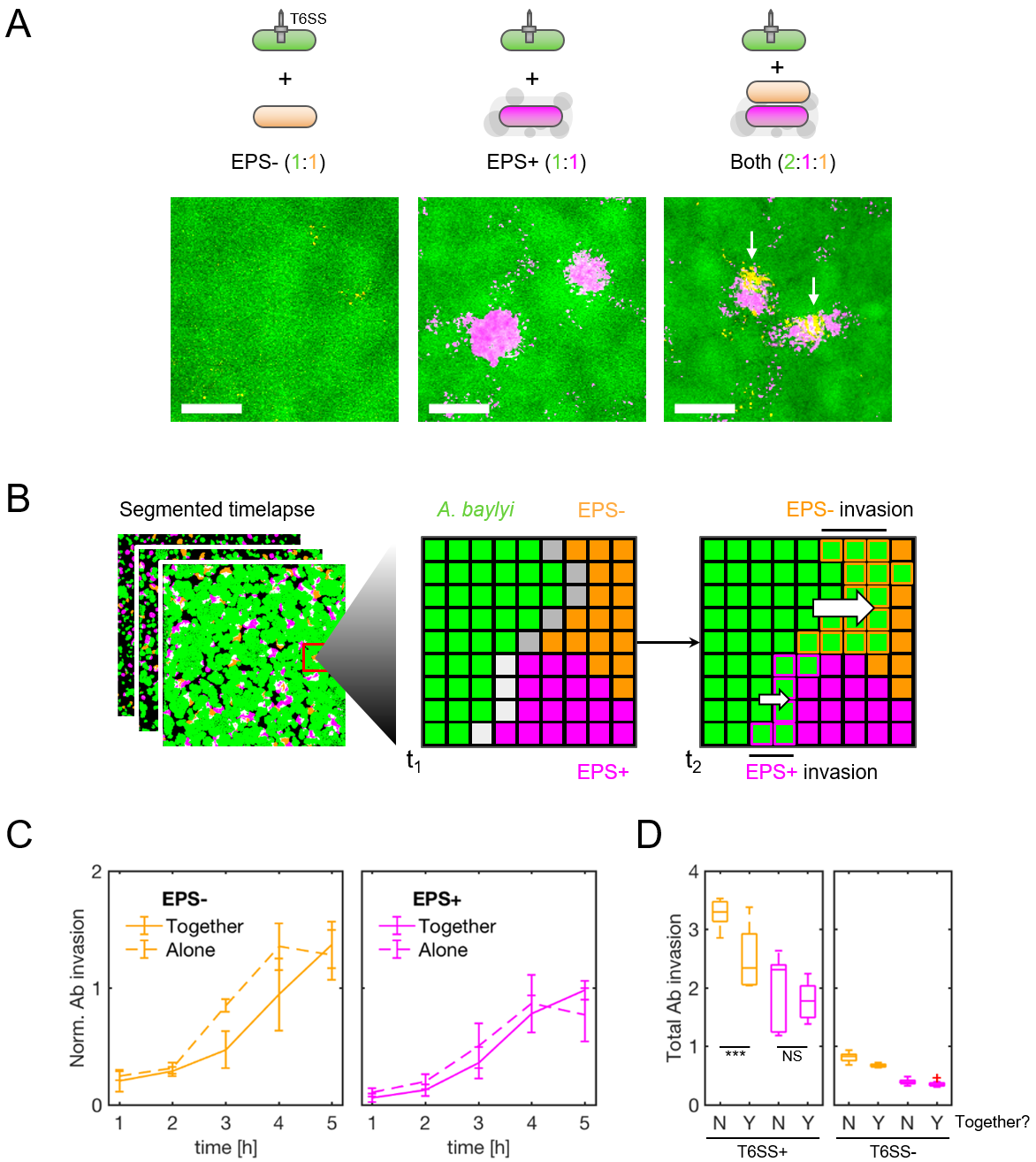

Fig. 4: *A. baylyi* invades EPS- *E. coli* cell groups less rapidly in the presence of EPS+ strain, supporting ranged protection via EPS sharing. (A) Attacker (green), EPS- (orange) and EPS+ (magenta) strains expressing fluorescent proteins were mixed and co-cultured as before (Fig. 2C,D), this time analysing competition dynamics using confocal microscopy. Colonies were imaged for 7h at 1h intervals, across five 470 x 470 µm frames spanning the colony edge (position 1) to its centre (position 5). Example images shown are zoomed-in areas of interest from position 4 (t = 6h); scale bars: 50 µm. **(B)** Automated image analysis for measuring rate of *A. baylyi* invasion into *E. coli* cell groups. We used segmented time-lapse images to identify i) boundaries between *A. baylyi* and EPS-, EPS+ *E. coli* cell groups (grey pixels), and ii) the rates at which *A. baylyi* expanded into EPS-, EPS+ *E. coli* groups

(orange- and magenta-edged pixels). **(C)** Measurements of *A. baylyi* invasion rates, normalised by boundary length, comparing invasion of EPS- (left) and EPS+ (right) cell groups, grown alone (dashed lines) or together (solid lines). Lines connect data means, and error bars denote standard deviations. Time-lapse data aggregated over colony positions 2-5; Position 1 was excluded for analysis since cells quickly grew beyond a monolayer, confounding our 2-D analysis. N=3 biological replicates; 12 data points per time point. (**D**) Comparison of total normalised invasion (area under curves in (D)) across all strain pairings, including T6SS- controls. Red cross denotes outlier data point (> Q3 + 1.5 * IQR). Significance assessed using one-sample Kruskal-Wallis tests; *** denotes p = 0.0004; N.S., non-significant.

DISCUSSION

Our modelling shows how EPS can serve as a highly protective, collective defence strategy against T6SS attacks, and one that can also mediate cross-protection of neighbouring, non-producing cells. Moreover, an experimental test of our model revealed that EPS dramatically increases *E. coli* survival in competition with T6SS-wielding *A. baylyi*. Here, colanic acid is secreted into the extracellular environment and we find evidence that it has the potential to protect cells other than the producer. Secretion of colanic acid is widespread in *Enterobacteriaceae* such as *E. coli*, *Klebsiella*, *Salmonella* and *Enterobacter* (40, 41), where it plays an important role in biofilm formation (35, 36, 42), and confers protection against various environmental stressors such as desiccation, osmotic stress, and oxidative stress (43, 44). Moreover, elevated EPS production (mucoidy) readily evolves in *E. coli* and other species in response to predation by phages (45–47), and membrane-anchored capsules can protect pathogenic bacteria from attacks by the immune system (48–50). EPS-mediated protection from T6SS attacks could therefore also evolve as a by-product of adaptation to other types of stressors, as well as a direct response to T6SS attacks itself.

With both modelling and experiments, we also found that EPS non-producing cells are able to survive T6SS attacks better when co-cultured with EPS producers. Additionally, our simulations identified a mechanism of cross-protection that we call flank protection, whereby groups of T6SS-resistant producers reduce the exposure of non-producers to attackers. However, in the experiments, we find evidence for a second, perhaps more intuitive, mechanism whereby loose EPS covers non-producers and directly shields them. Specifically, our microscopy experiments support the presence of direct protection via EPS sharing, as evidenced by a reduction in attacker invasion at the edges of non-producer cell groups. This implies that secreted EPS can shield non-producing cells, at a range spanning multiple cell lengths.

As discussed, our analyses do not exclude flank protection as a contributor to cross-protection in our experiments; we expect it to occur in parallel with EPS sharing. Indeed, flank protection has

290 the potential to be highly general: it is predicted to emerge whenever sensitive cell groups
291 interface with resistant cell groups, without assuming anything about the underlying resistance
292 mechanism. Collective resistance, therefore, may emerge widely, including in cases where EPS
293 is not shared between cells (15). More generally, flank protection has the potential to be mediated
294 by other mechanisms of T6SS resistance, such as envelope stress responses, or the production
295 of immunity proteins. In principle, it could generate unexpected collective protection against any
296 contact-dependent weapon, including via the T4SS, T7SS, and Cdi systems (4), adding further
297 complexity to interbacterial interactions.
298
299 T6SS-wielding bacteria are increasingly being considered as potential biotherapeutics, capable
300 of delivering toxins into pathogenic bacteria (51, 52). Our work cautions that many species have
301 the potential to resist such attacks due to the widespread ability of bacteria to work as collectives.
302 Consistent with this, bacteria are already known to display collective defences against antibiotics
303 (17, 19, 22), predators (53) and phage (20), and biofilm formation continues to be a major issue
304 in industry and medicine (54–57). Strategies that seek to remove problem strains, therefore,
305 needs to consider the ability of bacteria to work both as individuals and as groups.
306

307 ## MATERIALS AND METHODS

308 ### Agent-based modelling

309 We ran agent-based model simulations using the open-source modelling software Cellmodeller
310 (58). To simulate T6SS-mediated interactions and EPS particle secretion, we devised additional
311 code modules, available for download at https://github.com/WilliamPJSmith/CellModeller. The
312 key processes incorporated in our model are summarised here.

313 Model description

314 *Cell growth and division*. Bacterial cells are modelled as exponentially-growing rigid elastic rods
315 with fixed radius R, which push on one another as they elongate and divide (after doubling their
316 initial volume V_0, plus a small random noise term η_{div}). All cells are assumed to have equal access
317 to growth-limiting nutrients. Generally, cells pay no growth penalty for using either T6SS needles
318 or EPS secretion, and so a cell's volume V increases over time as $\Delta V = k_{grow} V \Delta t$, with k_{grow} the
319 maximum specific growth rate, and Δt the simulation timestep. However, we also explored
320 scenarios in which EPS secretion carried a range of growth costs proportional to the EPS
321 secretion rate (see Fig. S2B,C). Immediately after cell growth, an energy penalty method is
322 applied each timestep to compute cell movements necessary to minimise total cell-cell overlap,

subject to viscous drag forces acting on each cell. This process, described previously in detail (23, 58), approximates the elastic repulsion forces acting between cells in physical contact.

EPS secretion. Similar to previous work, we model agglomerations of EPS polymers as inert, pseudospherical particles (29–31). EPS+ cells secrete these particles from randomly chosen points on their surface. These particles have radius 0.4 μm, rod segment length 0.01 μm, and are assumed mechanically identical to bacterial cells. The secretion probability per time step, P_{EPS}, is at most 0.1, such that the max secretion rate is capped at 1 particle per timestep. EPS particles persist indefinitely, and completely ignore the effects of T6SS toxin injection (see below).

T6SS interactions. Each time step, T6SS+ cells can fire needles of length *R/2,* projecting orthogonally from randomly chosen sites on their cell surface. The number of firings per cell per unit time is drawn from a Poisson distribution, whose mean is k_{fire}. After firing, each needle is checked to determine if it comes into contact with any other cell in the population (line-segment method). Subsequent to this contact finding, each cell's state is updated to indicate the number of T6SS needle hits it sustained. Cells die (cease growing) after being struck N_{hits} times in this way, and lyse (disappear) following a fixed delay of $1 / k_{lysis}$. Each T6SS needle can deliver its toxin payload to at most one cell. T6SS+ cells are assumed completely immune to their own T6SS toxins, such that they effectively ignore all collateral fire from clone-mates. EPS particles do not obstruct T6SS needles, and so EPS particles can only protect bacterial cells from T6SS attacks by enforcing spatial separation of attacker and susceptible cells.

Computation and post-processing

All agent-based simulations were run using a 2017 Apple MacBook Pro laptop computer, with concurrent simulations distributed between an Intel 3.1 GHz quadcore i7-7920HQ CPU, an Intel HD 630 Graphics card, and an AMD Radeon Pro 560 Compute Engine. Simulation data were visualised using Paraview software, and analysed using custom Matlab and R scripts.

Simulation protocols

All simulations were initialised by randomly scattering different combinations of cells on a flat surface, within a circular 'homeland' of radius 50 μm. At simulation time $t = 0$, all cells lie flat on the surface, but have randomised orientations. All simulations were run for 130 time steps (Δt = 0.025h), totalling 3.25h of simulated time. Depending on conditions (most crucially, the number of EPS particles present), most simulations had a runtime of between 10 and 30 minutes (approximately 10 simulations per hour after concurrency).

355 **Bacterial growth conditions**

356 All strains were routinely grown overnight in 5 ml LB medium (per L: 10g Tryptone, 10g NaCl, 5g
357 Yeast Extract) in 15 mL polypropylene tubes with agitation (220 rpm). Where necessary, the
358 medium was supplemented with streptomycin (50 µg/mL), ampicillin (100 µg/mL), carbenicillin
359 (100 µg/mL) or gentamycin (15 µg/mL). Routine culturing was carried out on 1.5% w/v LB Agar
360 at 37°C (*E. coli*) or 30°C (*A. baylyi*). All pre-cultures and experiments were carried out at 30°C on
361 0.8% w/v LB Agar, unless indicated otherwise. Optical density (OD) of liquid cultures was
362 measured at 600 nm. For time-lapse microscopy experiments, samples were kept at 30°C
363 throughout the duration of the experiment using a custom-built incubation chamber.

364

365 **Strain construction**

366 For the generation of MG1655 *mScarlet-I*::Tn7 and MG1655 *mTagBFP2*::Tn7, MG1655 cells were
367 transformed with either pGRG25-P*max*::*mScarlet-I* or pGRG25-P*max*::*mTagBFP2* via
368 electroporation and selected on ampicillin at 30°C. The resulting transformants were cultured for
369 16 h at 30°C in liquid LB medium supplemented with ampicillin and arabinose (0.5% w/v). A small
370 volume (appr. 5 µL) of these cultures was streaked onto 1.5% w/v LB agar supplemented with
371 arabinose (0.5% w/v) and incubated at 42°C for 12 h. For each construct, three fluorescent
372 colonies were then selected, streaked onto 1.5% w/v LB agar and incubated at 42°C for 12 h.
373 Resulting colonies were tested for ampicillin sensitivity. For the generation of *E. coli* MG1655
374 *mScarlet-I*::Tn7 pRcsA2, MG1655 *mScarlet-I*::Tn7 cells were transformed with pRcsA2 (37) via
375 electroporation and selected on 100 µg/mL carbenicillin at 37°C. All plasmids and strains used in
376 this study are listed in Table S2.

377

378 **Competition assays**

379 To monitor survival of different *E. coli* strains in competition with *A. baylyi* strains, overnight
380 cultures of *A. baylyi* and *E. coli* were diluted (*A. baylyi* 1:10; *E. coli* 1:100) into 5 mL of fresh LB
381 medium supplemented with appropriate antibiotics (Table S2) and 0.5 mM IPTG to induce
382 production of colanic acid. We used *vipA-sfGFP*-labelled *A. baylyi* ADP1 as the T6SS-positive
383 competitor, whereas an isogenic *tssM* deletion mutant was used as T6SS-negative control
384 competitor. Cultures were then grown for 3 h with agitation, washed twice with LB medium, and
385 resuspended and normalized in LB medium to an optical density at 600 nm (OD600) of 0.1. An
386 *A. baylyi* strain was then mixed with an *E. coli* strain at a ratio of 1:1 (100 µL : 100 µL), and for

387 each strain combination 5 µL were spotted in triplicates in 24-well plates pre-filled with LB agar
388 supplemented with 0.5 mM IPTG (1 mL per well). For experiments at different seeding densities
389 (Fig. 2), the initial 1:1 mix was further diluted 10-fold (for OD = 0.01) or 100-fold (for OD = 0.001)
390 before being spotted on LB agar. For experiments with three competitors (Fig. 2), one *A. baylyi*
391 strain and two *E. coli* strains were normalized to OD = 0.1, mixed at a ratio of 2:1:1 (*A. baylyi* : *E.*
392 *coli* : *E. coli*), and further diluted if required before being spotted on LB agar. Plates were then
393 dried in a laminar flow at room temperature for approximately 20 min to allow droplet drying,
394 before being incubated at 30°C for 6 h. After incubation, competition spots were washed off with
395 500 µL NaCl (0.8%) each and subjected to seven rounds of 10-fold serial dilution. Colony-forming
396 units (CFUs) of *A. baylyi* and *E. coli* strains were determined by plating on streptomycin (100
397 µg/mL; selecting for *A. baylyi*), ampicillin/carbenicillin (100 µg/mL; selecting for *E. coli* MG1655
398 pRcsA2) or gentamycin (15 µg/mL; selecting for *E. coli* MG1655 Gen^R) media, incubated at 30°C
399 (*A. baylyi*) or 37°C (*E. coli*).
400

401 **Determination of T6SS firing rate**

402 To determine T6SS firing rate in *A. baylyi* cells exposed to EPS produced by *E. coli* (Fig. S4A),
403 cells of *E. coli* EPS+ and EPS- were grown overnight for 16 hours at 37°C, and 1 mL of bacterial
404 suspension was centrifuged for 5 min at 17000 g to sediment cells. The resulting supernatants
405 were sterile-filtered using 0.2 µm syringe filters (Sartorius), and 5 µL were each pipetted onto
406 separate cut-outs (ca. 5 mm x 5 mm) of 1% w/v LB agarose and left to dry for 20 min at room
407 temperature. In parallel, cells of the focal strain (*A. baylyi* T6SS+ *clpV-mCherry2*) were grown to
408 exponential phase in liquid culture (OD600 ~ 0.8-1.0) before spotting 1 µL of culture onto the
409 agarose pads treated with supernatant, and leaving them to dry for 5 min at room temperature.
410 Pads were then inverted onto a 5-cm diameter glass bottom Petri dish with a 3-cm diameter
411 uncoated n° 1.5 glass window (MatTek Corporation), so that the cells were sandwiched between
412 the agarose and the glass. The sample was then moved to the microscope and imaged
413 immediately. Time-lapse fluorescence microscopy was performed using a Zeiss Axio Observer
414 inverted microscope with a Zeiss Plan-Apochromat 63x oil immersion objective (NA = 1.4) and
415 ZEN Blue software (version 1.1.2.0). Time-lapse images were recorded for 3 minutes at a 10-
416 second interval. Exposure times were 1.05 ms for brightfield and 500 ms for mCherry2 (ex:
417 589 nm | em: 610 nm). The rate of T6SS firing was measured in a total of n = 916 *A. baylyi* cells
418 via detection of ClpV (*mCherry*) fluorescent foci (24). Each new ClpV focus was assumed to mark
419 one T6SS contraction event in a focal cell. Three separate fields of view at different locations on

420 the same agarose pad were monitored for each treatment. Image analysis was performed using
421 FIJI 2.1.0/1.53c (59). For each field of view, total number of cells and ClpV foci were determined
422 each minute via thresholding, segmentation and object counting in the brightfield channel, and
423 the FIJI built-in “Find maxima” function in the mCherry fluorescence channel, respectively

424

425 **Colanic acid quantification**

426 To quantify the amount of colanic acid (CA) produced by different *E. coli* strains (Fig. S2), 1 mL
427 of overnight cultures were washed once with fresh LB medium and density-adjusted to an OD of
428 1.0. For each strain, 50 µL were then spotted in triplicates in 24-well plates pre-filled with LB agar
429 supplemented with 0.5 mM IPTG (1 mL per well). Plates were then dried in a laminar flow at room
430 temperature for approximately 20 min to allow droplet evaporation, before being incubated at
431 30°C for 6h. Cell material was then harvested by adding 1 mL of sterile ddH_2O to the well and
432 pipetting up and down until all material was suspended, and then transferred to a sterile 1.5 mL
433 tube. Tubes were vortexed for 5-7 seconds, and the OD600 was determined for all replicates. Of
434 these volumes, twice 400 µL were then transferred to two separate reaction tubes pre-filled with
435 600 µL ddH_2O: one for quantification of total CA, and one for quantification of CA secreted into
436 the extracellular environment. For quantification of total CA (Fig. S3), samples were boiled for 20
437 min at 95°C, centrifuged at 17’000 g for 20 min, and 1 mL of supernatant was used for further
438 processing. For quantification of CA in the extracellular environment (Fig. S3), samples were
439 centrifuged at 17’000 g for 20 min, and 1 mL of supernatant was used for further processing. To
440 test whether sterile-filtering removes EPS from supernatants (Fig. S4B), *E. coli* MG1655 pRcsA2
441 (EPS+) and MG1655 Gen^R (EPS-) strains were grown overnight for 16 hours at 37°C, and 1 mL
442 of bacterial suspension was centrifuged for 5 min at 17000 g to sediment cells. The resulting
443 supernatants were either sterile-filtered using 0.2 µm syringe filters (Sartorius) or left unfiltered,
444 and 900uL of supernatant was used for further processing. Relative CA production was then
445 determined through the quantification of L-Fucose (60). Briefly, samples were boiled with 4.5 mL
446 $H_2SO_4 \cdot H_2O$ (6:1 H_2SO_4 and H_2O) for 20 min and cooled to room temperature. Then, 900 µL of
447 each sample was transferred to a spectrophotometer cuvette and absorbance was measured at
448 396 nm (A_{396}) and 427 nm (A_{427}). To each cuvette was then added 100 µL of freshly prepared L-
449 cysteine hydrochloride (1M), mixed by pipetting, and absorbance was again measured at 396 nm
450 ($A\text{-}cy_{396}$) and 427 nm ($A\text{-}cy_{427}$). The concentration of L-Fucose was then determined by calculating

451 $(A\text{-}cy_{396} - A_{396}) - (A\text{-}cy_{427} - (A_{427})$ and applying a previously generated L-Fucose standard
452 curve (0-100 µg/mL).
453
454 **Confocal microscopy**
455 To image competition dynamics, fluorescently tagged versions of all relevant strains (Table S2)
456 were pre-cultured and density-adjusted to OD600 = 0.1 as described in "Competition assays".
457 For each strain combination, 5 µL were then spotted onto a glass bottom Petri dish filled with 8
458 mL 0.8% w/v LB agar supplemented with 0.5 mM IPTG. After drying for ten minutes at room
459 temperature, the plate was inverted to allow for immediate imaging of the competition area
460 through air. Time-lapse confocal imaging was then carried out using a Zeiss Plan-Apochromat
461 10x objective (NA = 0.45) on a Zeiss LSM880 confocal laser scanning unit using ZEN Black
462 software (version 14.0.18.201). Images (each covering an area of 472.33 µm x 472.33 µm) were
463 acquired hourly for 7 h, over 5 different colony positions, spanning in total the entire radius of the
464 competition area (edge to centre). Three biological replicates were carried out for each strain
465 combination.
466
467 **Confocal image analysis**
468 *Image segmentation and stabilization.* Following acquisition, raw confocal image data were
469 analyzed using FIJI (59). Multichannel images were split into individual channels, with each
470 channel subjected to separate background subtraction (rolling ball radius 50 px) and conversion
471 to binary image data via user-defined thresholds. To maximise the accuracy of cell group
472 boundary tracking, we stabilised images using the FIJI 'StackReg' plugin (61), applied to the GFP
473 (*A. baylyi*) channel. This stabilisation made it necessary to exclude later time points (t=6,7h) as
474 these were typically confluent, confounding accurate registration of images. We also excluded
475 colony position 1 (colony edge); here, coffee-ring effects (62) consistently led to the formation of
476 3-D cell groups as early as 2h into the competition. As our image analysis is limited to 2-D, we
477 were unable to accurately track inter-strain boundaries at this position. For visualization purposes,
478 mtagBFP2 fluorescence is false-coloured orange in all images throughout the manuscript.
479
480 *Normalised invasion rates*. To estimate T6SS killing rates at interstrain boundaries (Fig. 4), we
481 tracked changes in strain occupancy at each pixel across consecutive time-lapse images, using

482 custom MATLAB scripts. We compared consecutive time points (t-1, t; t=1,2,3,4,5h) in each
483 stablised time lapse. Any pixel where EPS+ channel signal was lost, and replaced with new *A.*
484 *baylyi* signal, was marked as being 'invaded' by *A. baylyi*, giving a measure of EPS+ cell killing
485 by the attacker. EPS+ invasion pixel counts were normalised by the amount of Ab-EPS+ contact
486 found in the t-1 image. We measured Ab-EPS+ contact by dilating *Ab* cell group images (MATLAB
487 *imdilate* method; 3 pixel spherical structuring element) and computing their overlap (in pixels) with
488 EPS+ cell groups. Performing this procedure in reverse (dilate EPS+ onto *Ab*) yielded similar
489 boundary pixel counts. EPS- invasion was calculated and normalised in the same way.

490

491 **Statistical Analysis**

492 Statistical analysis and data visualization were performed using RStudio version 1.2.5033 (63)
493 and packages dplyr (64), Rmisc (65), ggplot2 (66), and cowplot (67); as well as Matlab version
494 2017b (9.3.0.713579). For all statistical tests, the significance level α was set to 0.05. To test
495 whether cell recovery differed between competitions (Fig. 2), two-way ANOVA of log-transformed
496 CFU values with a post-hoc Tukey's HSD test was performed. To test whether colanic acid
497 production differed between strains (Fig. S3B), and whether firing rate differed when cells were
498 exposed to EPS (Fig. S4A), a two-sided Wilcoxon rank sum test was performed. To test whether
499 filtering removed EPS from supernatants (Fig. S4B), a two-sided, paired samples Wilcoxon signed
500 rank test was performed. To test whether total normalised invasion of the EPS- strain changed
501 when grown alongside the EPS+ strain (or vice versa; Fig. 4), we used one-sample Kruskal-Wallis
502 tests. Statistical details (sample size, test values, p-values) for each experiment are provided in
503 the respective Figure legends.

504

505 **ACKNOWLEDGEMENTS**

506 We thank Marek Basler, Colin Kleanthous and Frances Spragge for strains, Chris French and
507 Thomas Meiller-Legrand for plasmids, and Erik Bakkeren, Ravinash Krishna Kumar, Jake Palmer,
508 and Rachel Wheatley for comments on the manuscript. ETG is funded by a Postdoc Mobility
509 Fellowship from the Swiss National Science Foundation (P400PB_183878) and a BBSRC
510 Discovery Fellowship (BB/V004328/1). WPJS and KRF are supported by the National Institutes
511 of Health (project numbers R01AI093771 and R01AI120633), by European Research Council
512 Grant 787932, and by Wellcome Trust Investigator award 209397/Z/17/Z. WPJS is also funded
513 by a Sir Henry Wellcome Postdoctoral fellowship award, 222795/Z/21/Z.

514 **REFERENCES**

515

516 1. M. Ghoul, S. Mitri, The Ecology and Evolution of Microbial Competition. *Trends Microbiol.*
517 **24**, 833–845 (2016).

518 2. M. E. Hibbing, C. Fuqua, M. R. Parsek, S. B. Peterson, Bacterial competition: Surviving
519 and thriving in the microbial jungle. *Nat. Rev. Microbiol.* **8**, 15–25 (2010).

520 3. J. D. Palmer, K. R. Foster, Bacterial species rarely work together. *Science* **376**, 581–582
521 (2022).

522 4. E. T. Granato, T. A. Meiller-Legrand, K. R. Foster, The Evolution and Ecology of Bacterial
523 Warfare. *Curr. Biol.* **29**, R521–R537 (2019).

524 5. S. B. Peterson, S. K. Bertolli, J. D. Mougous, The Central Role of Interbacterial
525 Antagonism in Bacterial Life. *Curr. Biol.* **30**, R1203–R1214 (2020).

526 6. F. R. Cianfanelli, L. Monlezun, S. J. Coulthurst, Aim, Load, Fire: The Type VI Secretion
527 System, a Bacterial Nanoweapon. *Trends Microbiol.* **24**, 51–62 (2016).

528 7. L. P. Allsopp, P. Bernal, L. M. Nolan, A. Filloux, Causalities of War: The connection
529 between T6SS and microbiota. *Cell. Microbiol.*, cmi.13153 (2019).

530 8. P. Bernal, L. P. Allsopp, A. Filloux, M. A. Llamas, The Pseudomonas putida T6SS is a
531 plant warden against phytopathogens. *ISME J.* **11**, 972–987 (2017).

532 9. C. Chen, X. Yang, X. Shen, Confirmed and Potential Roles of Bacterial T6SSs in the
533 Intestinal Ecosystem. *Front. Microbiol.* **0** (2019).

534 10. R. Gallegos-Monterrosa, S. J. Coulthurst, The ecological impact of a bacterial weapon:
535 microbial interactions and the Type VI secretion system. *FEMS Microbiol. Rev.* (2021).

536 11. B. Chassaing, E. Cascales, Antibacterial Weapons: Targeted Destruction in the Microbiota.
537 *Trends Microbiol.* **26**, 329–338 (2018).

538 12. N. Flaugnatti, *et al.*, Human commensal gut Proteobacteria withstand type VI secretion
539 attacks through immunity protein-independent mechanisms. *Nat. Commun.* **12**, 5751
540 (2021).

541 13. S. J. Hersch, *et al.*, Envelope stress responses defend against type six secretion system
542 attacks independently of immunity proteins. *Nat. Microbiol.* **5**, 706–714 (2020).

543 14. S. Robitaille, E. Trus, B. D. Ross, Bacterial Defense against the Type VI Secretion System.
544 *Trends Microbiol.* (2020) https:/doi.org/10.1016/j.tim.2020.09.001 (November 22, 2020).

545 15. J. Toska, B. T. Ho, J. J. Mekalanos, Exopolysaccharide protects Vibrio cholerae from
546 exogenous attacks by the type 6 secretion system. *Proc. Natl. Acad. Sci.*, 201808469
547 (2018).

548 16. S. J. Hersch, K. Manera, T. G. Dong, Defending against the Type Six Secretion System:
549 beyond Immunity Genes. *Cell Rep.* **33**, 108259 (2020).

550 17. I. Frost, *et al.*, Cooperation, competition and antibiotic resistance in bacterial colonies.
551 *ISME J.* **12**, 1582–1593 (2018).

552 18. E. T. Granato, K. R. Foster, The Evolution of Mass Cell Suicide in Bacterial Warfare. *Curr.*
553 *Biol.* (2020) https:/doi.org/10.1016/j.cub.2020.05.007 (June 5, 2020).

554 19. R. Krishna Kumar, *et al.*, Droplet printing reveals the importance of micron-scale structure
555 for bacterial ecology. *Nat. Commun.* **12**, 857 (2021).

556 20. A. Lopatina, N. Tal, R. Sorek, Abortive Infection: Bacterial Suicide as an Antiviral Immune
557 Strategy. *Annu. Rev. Virol.* **7**, 371–384 (2020).

558 21. D. A. I. Mavridou, D. Gonzalez, W. Kim, S. A. West, K. R. Foster, Bacteria Use Collective
559 Behavior to Generate Diverse Combat Strategies. *Curr. Biol.* **28**, 345-355.e4 (2018).

560 22. D. A. C. Stapels, *et al.*, Salmonella persisters undermine host immune defenses during
561 antibiotic treatment. *Science* **362**, 1156–1160 (2018).

562 23. W. P. J. Smith, *et al.*, Cell morphology drives spatial patterning in microbial communities.
563 *Proc. Natl. Acad. Sci. U. S. A.* **114**, E280–E286 (2017).

564 24. W. P. J. Smith, *et al.*, The evolution of the type VI secretion system as a disintegration
565 weapon. *PLOS Biol.* **18**, e3000720 (2020).

566 25. W. P. J. Smith, *et al.*, The evolution of tit-for-tat in bacteria via the type VI secretion
567 system. *Nat. Commun.* **11**, 5395 (2020).

568 26. H.-C. Flemming, J. Wingender, The biofilm matrix. *Nat. Rev. Microbiol.* **8**, 623–633 (2010).

569 27. H. C. Flemming, S. Wuertz, Bacteria and archaea on Earth and their abundance in
570 biofilms. *Nat. Rev. Microbiol.* **17**, 247–260 (2019).

571 28. B. Lories, *et al.*, Biofilm Bacteria Use Stress Responses to Detect and Respond to
572 Competitors. *Curr. Biol.* **30**, 1231-1244.e4 (2020).

573 29. P. Ghosh, J. Mondal, E. Ben-Jacob, H. Levine, Mechanically-driven phase separation in a
574 growing bacterial colony. *Proc. Natl. Acad. Sci.* **112**, E2166–E2173 (2015).

575 30. J. U. Kreft, J. W. Wimpenny, Effect of EPS on biofilm structure and function as revealed by
576 an individual-based model of biofilm growth. *Water Sci. Technol. J. Int. Assoc. Water*
577 *Pollut. Res.* **43**, 135–141 (2001).

578 31. J. B. Xavier, K. R. Foster, Cooperation and conflict in microbial biofilms. *Proc. Natl. Acad.*
579 *Sci.* **104**, 876–881 (2007).

580 32. A. Berdahl, C. J. Torney, C. C. Ioannou, J. J. Faria, I. D. Couzin, Emergent Sensing of
581 Complex Environments by Mobile Animal Groups. *Science* **339**, 574–576 (2013).

582 33. D. B. Borenstein, P. Ringel, M. Basler, N. S. Wingreen, Established Microbial Colonies
583 Can Survive Type VI Secretion Assault. *PLOS Comput. Biol.* **11**, e1004520 (2015).

584 34. P. D. Ringel, D. Hu, M. Basler, The Role of Type VI Secretion System Effectors in Target
585 Cell Lysis and Subsequent Horizontal Gene Transfer. *Cell Rep.* **21**, 3927–3940 (2017).

586 35. P. N. Danese, L. A. Pratt, R. Kolter, Exopolysaccharide Production Is Required for
587 Development of Escherichia coli K-12 Biofilm Architecture. *J. Bacteriol.* (2000)
588 https:/doi.org/10.1128/JB.182.12.3593-3596.2000 (December 28, 2021).

589 36. M. Horvat, A. Pannuri, T. Romeo, I. Dogsa, D. Stopar, Viscoelastic response of
590 Escherichia coli biofilms to genetically altered expression of extracellular matrix
591 components. *Soft Matter* **15**, 5042–5051 (2019).

592 37. N. Joshi, B. T. Ngwenya, C. E. French, Enhanced resistance to nanoparticle toxicity is
593 conferred by overproduction of extracellular polymeric substances. *J. Hazard. Mater.* **241–**
594 **242**, 363–370 (2012).

595 38. C. Whitfield, Biosynthesis and Assembly of Capsular Polysaccharides in Escherichia coli.
596 *Annu. Rev. Biochem.* **75**, 39–68 (2006).

597 39. J. van Gestel, F. J. Weissing, O. P. Kuipers, Á. T. Kovács, Density of founder cells affects
598 spatial pattern formation and cooperation in Bacillus subtilis biofilms. *ISME J.* **8**, 2069–
599 2079 (2014).

600 40. M. Rättö, *et al.*, Colanic acid is an exopolysaccharide common to many enterobacteria
601 isolated from paper-machine slimes. *J. Ind. Microbiol. Biotechnol.* **33**, 359–367 (2006).

602 41. C. Sande, C. Whitfield, Capsules and Extracellular Polysaccharides in Escherichia coli and
603 Salmonella. *EcoSal Plus* **9**, eESP-0033-2020 (2021).

604 42. M. M. Hahn, J. S. Gunn, Salmonella Extracellular Polymeric Substances Modulate Innate
605 Phagocyte Activity and Enhance Tolerance of Biofilm-Associated Bacteria to Oxidative
606 Stress. *Microorganisms* **8**, 253 (2020).

607 43. J. Chen, S. M. Lee, Y. Mao, Protective effect of exopolysaccharide colanic acid of
608 Escherichia coli O157:H7 to osmotic and oxidative stress. *Int. J. Food Microbiol.* **93**, 281–
609 286 (2004).

610 44. T. Ophir, D. L. Gutnick, A role for exopolysaccharides in the protection of microorganisms
611 from desiccation. *Appl. Environ. Microbiol.* **60**, 740–745 (1994).

612 45. K. Mizoguchi, *et al.*, Coevolution of Bacteriophage PP01 and Escherichia coli O157:H7 in
613 Continuous Culture. *Appl. Environ. Microbiol.* **69**, 170–176 (2003).

614 46. P. D. Scanlan, A. Buckling, Co-evolution with lytic phage selects for the mucoid phenotype
615 of Pseudomonas fluorescens SBW25. *ISME J.* **6**, 1148–1158 (2012).

616 47. S. Wielgoss, T. Bergmiller, A. M. Bischofberger, A. R. Hall, Adaptation to Parasites and
617 Costs of Parasite Resistance in Mutator and Nonmutator Bacteria. *Mol. Biol. Evol.* **33**,
618 770–782 (2016).

619 48. P. Domenico, R. J. Salo, A. S. Cross, B. A. Cunha, Polysaccharide capsule-mediated
620 resistance to opsonophagocytosis in Klebsiella pneumoniae. *Infect. Immun.* **62**, 4495–
621 4499 (1994).

622 49. T. A. Russo, *et al.*, The K1 capsular polysaccharide of Acinetobacter baumannii strain 307-
623 0294 is a major virulence factor. *Infect. Immun.* **78**, 3993–4000 (2010).

624 50. M. R. Wessels, A. E. Moses, J. B. Goldberg, T. J. DiCesare, Hyaluronic acid capsule is a
625 virulence factor for mucoid group A streptococci. *Proc. Natl. Acad. Sci.* **88**, 8317–8321
626 (1991).

627 51. M. Raffatellu, Learning from bacterial competition in the host to develop antimicrobials.
628 *Nat. Med.* **24**, 1097–1103 (2018).

629 52. C. Rüter, P. R. Hardwidge, 'Drugs from Bugs': bacterial effector proteins as promising
630 biological (immune-) therapeutics. *FEMS Microbiol. Lett.* **351**, 126–132 (2014).

631 53. G. Corno, K. Jürgens, Direct and Indirect Effects of Protist Predation on Population Size
632 Structure of a Bacterial Strain with High Phenotypic Plasticity. *Appl. Environ. Microbiol.* **72**,
633 78–86 (2006).

634 54. R. M. Donlan, J. W. Costerton, Biofilms: Survival Mechanisms of Clinically Relevant
635 Microorganisms. *Clin. Microbiol. Rev.* **15**, 167–193 (2002).

636 55. A. Schulze, F. Mitterer, J. P. Pombo, S. Schild, Biofilms by bacterial human pathogens:
637 Clinical relevance – development, composition and regulation – therapeutical strategies.
638 *Microb. Cell* **8**, 28–56 (2021).

639 56. M. Jamal, *et al.*, Bacterial biofilm and associated infections. *J. Chin. Med. Assoc. JCMA*
640 **81**, 7–11 (2018).

641 57. S. Galié, C. García-Gutiérrez, E. M. Miguélez, C. J. Villar, F. Lombó, Biofilms in the Food
642 Industry: Health Aspects and Control Methods. *Front. Microbiol.* **9** (2018).

643 58. T. J. Rudge, P. J. Steiner, A. Phillips, J. Haseloff, Computational modeling of synthetic
644 microbial biofilms. *ACS Synth. Biol.* **1**, 345–352 (2012).

645 59. J. Schindelin, *et al.*, Fiji: An open-source platform for biological-image analysis. *Nat.*
646 *Methods* **9**, 676–682 (2012).

647 60. B. Obadia, *et al.*, Influence of Tyrosine-Kinase Wzc Activity on Colanic Acid Production in
648 Escherichia coli K12 Cells. *J. Mol. Biol.* **367**, 42–53 (2007).

649 61. P. Thevenaz, U. E. Ruttimann, M. Unser, A pyramid approach to subpixel registration
650 based on intensity. *IEEE Trans. Image Process.* **7**, 27–41 (1998).

651 62. A. Agrawal, S. Sinha, R. Mukherjee, D. Mampallil, Dynamics of bacterial deposition in
652 evaporating drops. *Phys. Fluids* **32**, 093308 (2020).

653 63. R Development Core Team, *R: A language and environment for statistical computing.* (R
654 Foundation for Statistical Computing, 2018).

64. L. H. and K. M. Hadley Wickham, Romain François, dplyr: A Grammar of Data Manipulation. R package version 0.7.6 (2018).

65. R. M. Hope, Rmisc: Ryan Miscellaneous. R package version 1.5. (2013).

66. P. M. Valero-Mora, *ggplot2: Elegant Graphics for Data Analysis* (Springer, 2010).

67. C. O. Wilke, cowplot: Streamlined Plot Theme and Plot Annotations for “ggplot2”. R package version 0.9.4. (2019).